

## Magnetic ordering in the presence of fast spin fluctuations: A neutron scattering study of $\text{CeIn}_3$

J. M. Lawrence

*Physics Department, University of California, Irvine, California 92717*

S. M. Shapiro

*Physics Department, Brookhaven National Laboratory, Upton, New York 11973*

(Received 28 January 1980)

We report results of elastic and inelastic neutron scattering experiments in the trivalent spin-fluctuation metal  $\text{CeIn}_3$ . Antiferromagnetic order occurs at  $10.23 \pm 0.01$  K. The magnetic reflections can be indexed on a doubled chemical cell of cubic symmetry. The saturated ordered moment  $0.65 \pm 0.1 \mu_B$  per cerium atom is comparable to the value  $0.71 \mu_B$  expected for ordering within the  $\Gamma_7$  doublet, which is the ground level expected for  $J = \frac{5}{2}$  cerium moments in a cubic crystal field. The critical behavior of the order parameter is of the form  $M_{\text{st}}^2(T)/M_{\text{st}}^2(0) = A[(T_N - T)/T_N]^{2\beta}$  where  $M_{\text{st}}$  is the staggered magnetization,  $A = 2.2 \pm 0.2$  and  $\beta = 0.42 \pm 0.02$ ; in addition the critical fluctuations are extremely weak. We discuss this nearly mean-field behavior in the context of recent theories which describe critical behavior in systems where the critical temperature is much smaller than a characteristic spin-fluctuation temperature. The inelastic scattering measurements provide evidence for the existence of such a characteristic energy. At low temperatures the inelastic cross section is dominated by an anomalously broad magnetic scattering peak, centered near 13 meV and with a half-width of about 10 meV. We interpret the large linewidth as arising from fast spin fluctuations, which arise from strong Kondo-type exchange coupling of the  $4f$  spins to the conduction electrons.

### I. INTRODUCTION

$\text{CeIn}_3$  is one of a class of rare-earth intermetallics whose physical properties reflect the simultaneous presence of magnetic interactions leading to magnetic order, crystal-field effects, and strong spin fluctuations due to the  $4f$  level being near the Fermi surface.<sup>1</sup> The lattice constant indicates that the material is trivalent.<sup>2</sup> However the Curie-Weiss susceptibility<sup>3</sup>  $\chi = C/(T + \theta)$  with large Weiss parameter  $\theta \approx 60$  K, the presence of a resistance minimum near 150 K,<sup>4</sup> and a very large linear heat capacity at low temperatures<sup>5</sup> all attest to the importance of low-energy spin fluctuations. Near 10 K the susceptibility shows a sharp cusp<sup>4</sup> indicating a phase transition into an antiferromagnetic ground state. Analysis of the susceptibility<sup>4</sup> and specific heat<sup>6</sup> suggests the presence of crystal-field effects.

It is the purpose of this paper to report microscopic confirmation of the above picture. In particular, we have established the microscopic character of the spin order by elastic neutron diffraction, and have studied the spin dynamics, in which the presence of spin fluctuations (and perhaps crystal fields) is reflected.

The low-temperature magnetic ordering which occurs in  $\text{CeIn}_3$  is unusual in that the ordering temperature ( $T_N \approx 10$  K) is much smaller than the spin-fluctuation temperature deduced from the thermo-

dynamic behavior [ $T_{\text{sf}} \approx 50-100$  K (Ref. 1)]. As has been shown in Ref. 1, when a small amount of tin is substituted for indium, the magnetic ground state is no longer stable, and the system no longer orders, i.e.,  $T_N(x) \rightarrow 0$  near  $x \approx 0.4$  in  $\text{CeIn}_{3-x}\text{Sn}_x$ . This means that the underlying energy parameters in  $\text{CeIn}_3$  lie near the values at which a magnetic-nonmagnetic instability of the  $4f$  electron occurs. Theoretically, an antiferromagnetic-nonmagnetic instability occurs in the one-dimensional Kondo-lattice model discussed by Doniach and co-workers.<sup>7</sup> While the relevance of this model to real mixed-valence materials has not been established, part of our purpose in this present study is to provide experimental input into the general problem of such an instability. Other recent theoretical work, by Beal-Monod<sup>8</sup> and Hertz<sup>9</sup> has examined the critical behavior for phase transitions occurring in systems with critical temperatures much smaller than characteristic quantum-mechanical energies (e.g.,  $T_N \ll T_{\text{sf}}$ ). As we will see below, the critical behavior of the  $\text{CeIn}_3$  phase transition seems to support those theories.

### II. EXPERIMENTAL DETAILS

#### A. Sample preparation and analysis

The polycrystalline samples were prepared by arc melting. Starting materials were: cerium and lantha-

num purchased from United Mineral and Chemical and quoted as 99.999% pure with respect to common metals; the indium was obtained from Materials Research Corp. and was Marz grade with 99.999% purity. To ensure homogeneity, several small (3 g) samples were initially prepared and homogenized by remelting. These were then melted together and remelted to form a single large sample.

Metallographic examination of polished surfaces of the large sample indicated that it consisted of large grains (100–300  $\mu\text{m}$  in diameter) of single-phase material, with minor inclusions of indium in the grain boundaries. We next examined small sections cut from the main boule using x-ray diffraction. All lines could be indexed on the  $\text{AuCu}_3$  crystal structure

and the room-temperature lattice constant (4.689  $\text{\AA}$ ) was in excellent agreement with earlier work.<sup>1</sup> These results were confirmed with Bragg scattering of neutrons, where  $a_0(10\text{ K}) = 4.633\text{ \AA}$ . An identically sized and shaped sample of  $\text{LaIn}_3$ , which was prepared to subtract the nuclear background in the neutron scattering, was also single-phase,  $\text{AuCu}_3$ -structured material, with  $a_0(300\text{ K}) = 4.728\text{ \AA}$ .

As a further check on sample quality we measured the magnetic susceptibility of a cylinder of material cut from the main boule. The results, exhibited in Fig. 1, are in excellent agreement with earlier work.<sup>1</sup> In particular the high-temperature Curie-Weiss behavior is identical with earlier results and the phase transition is extremely sharp. The latter serves as an important check, since inhomogeneity would be manifest in a rounding of the transition.

For the study of the temperature dependence of the order parameter, a large single crystal (1 cm in diameter and 1 cm long) was used. This was grown at the University of Rochester by a modified Bridgman technique. The crystal was twinned, consisting of two large grains and a plethora of small crystallites near the bottom surface. The angle between the twins was of order  $10^\circ$ . The mosaic of the grain used was slightly asymmetric with less than  $0.6^\circ$  full width at half maximum (FWHM). This sample was used solely for measurements of the temperature dependence of the magnetic reflections.

## B. Neutron experiments

### 1. Polycrystalline scattering

The neutron experiments were carried out at the Brookhaven High Flux Beam Reactor. Pyrolytic graphite (PG) monochromator and analyzer crystals were used throughout the experiment. Initial studies were performed on solid slab-shaped polycrystalline materials of dimensions  $0.32 \times 1.27 \times 2.54\text{ cm}^3$  and  $0.14 \times 1.27 \times 2.54\text{ cm}^3$ . There was considerable preferred orientation in these samples due to the large grain size. The neutron data reported below for polycrystalline samples were obtained on samples which were powdered in a flowing-helium atmosphere in a drybox. The dust was then loaded into a thin-walled aluminum container with interior dimensions  $0.127 \times 1.59 \times 2.5\text{ cm}^3$  and with a wall thickness 0.15 cm. This container was mounted in an aluminum can, filled with helium gas to increase the heat transfer, and then placed on the cold finger of a conventional cryostat. (The identically sized and shaped  $\text{LaIn}_3$  sample was treated similarly.) A check for preferred orientation in the powder was performed by rotating the sample with the scattering angle set for the Bragg condition; within the statistics, preferred orientation was negligible. However, the discrepancy of order

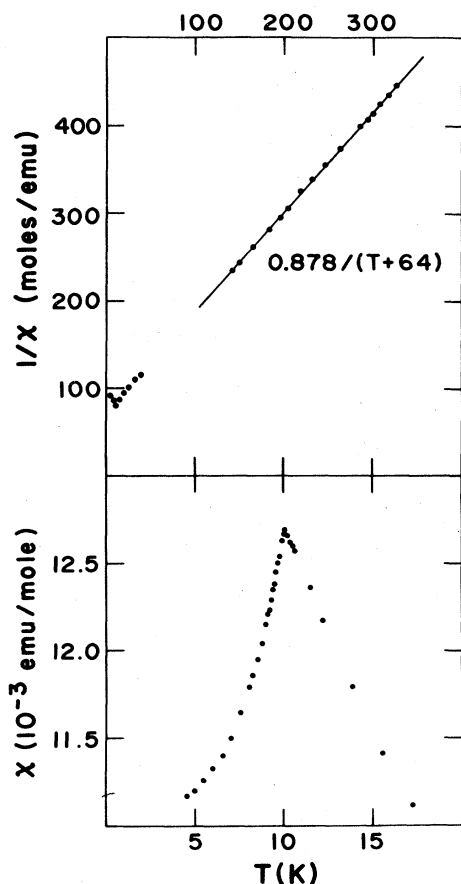


FIG. 1. (a) The inverse dc susceptibility of  $\text{CeIn}_3$ , measured on a sample cut from the same boule as used in the neutron studies. Both the high-temperature Curie-Weiss behavior, which is characteristic of spin-fluctuation metals, and the antiferromagnetic transition near 10 K are apparent in this plot. The units of the Curie constant are  $\text{emu} \times \text{K}/\text{mole}$ . (b) The dc susceptibility of  $\text{CeIn}_3$  near the antiferromagnetic phase transition. The sharpness of the cusp is related to the weakness of the critical fluctuations in this system.

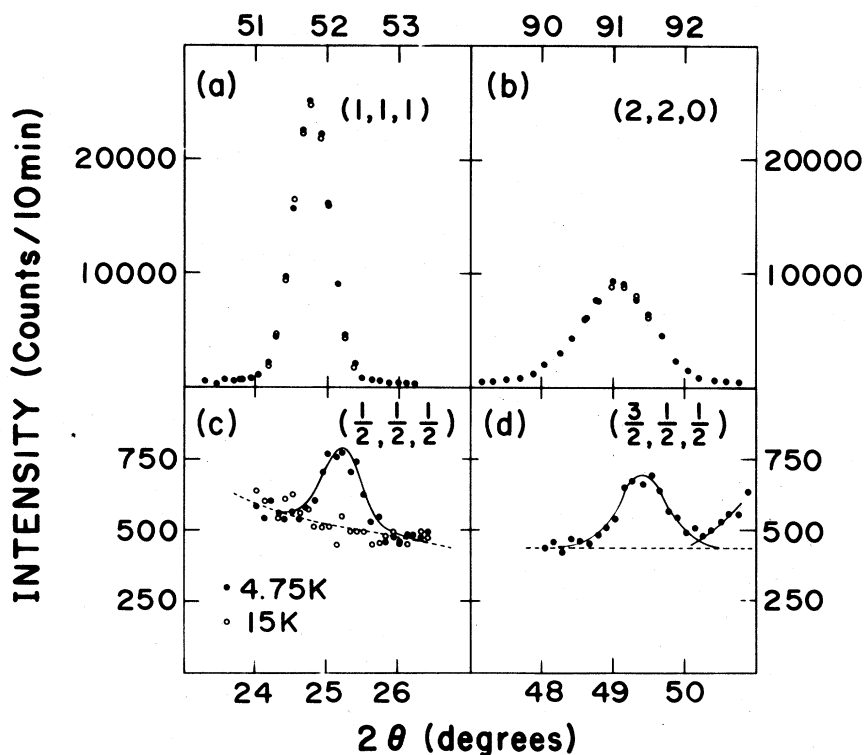


FIG. 2. Scattering intensity vs Bragg angle for polycrystalline  $\text{CeIn}_3$  at  $T = 4.75$  K (closed circles) and  $T = 15$  K (open circles) for the: (a)  $(1,1,1)$  nuclear peak; (b) the  $(2,2,0)$  nuclear peak; (c) the  $(\frac{1}{2}, \frac{1}{2}, \frac{1}{2})$  magnetic reflection; and (d) the  $(\frac{3}{2}, \frac{1}{2}, \frac{1}{2})$  magnetic reflection. The dashed lines in (c) and (d) represent a smooth fit to the background and the solid lines represent a smooth fit to the magnetic scattering. The upturn above  $2\theta = 50.2^\circ$  in (d) represents the low angle tail of the  $(1,1,1)$  reflection.

20% in the ratio of the magnitudes of the  $(1,1,1)$  and  $(2,2,0)$  nuclear peaks (Fig. 2) arises in part from granularity and gives a better indication of the degree of this effect.

Bragg scattering was performed with an incident neutron energy of 14.8 meV; the horizontal collimation was  $40'-40'-40'-40'$  between the reactor and monochromator, monochromator and sample, sample and analyzer, and the analyzer and detector, respectively. A PG filter was placed before the monochromator to eliminate higher-order contamination. The Bragg spectra consisted of both the expected  $\text{CeIn}_3$  lines, and lines from the aluminum sample holder of comparable intensity; there was no contribution from free indium. In addition there were two weak impurity lines at  $Q = 0.49$  and  $1.78 \text{ \AA}^{-1}$ , whose intensity was 0.5% of that of the  $\text{CeIn}_3$   $(1,1,1)$  peak and which could not be indexed on any known oxide or hydride phase of cerium. Since the scattering lengths of cerium and indium are nearly equal ( $b_{\text{Ce}} = 0.48 \times 10^{-12}$  cm,  $b_{\text{In}} = 0.39 \times 10^{-12}$  cm, and  $b_{\text{La}} = 0.83 \times 10^{-12}$  cm) (Ref. 10) only (even, even, even) and (odd, odd, odd) reflections were observed in  $\text{CeIn}_3$ .

The inelastic scattering was performed in the constant  $Q$  mode with fixed final energy of 30 meV and

with horizontal collimation  $40'-20'-40'-40'$ . No PG filter was used. A monitor was placed just before the sample. In this configuration no correction factor is needed to account for variations in instrumental resolution as the energy varies.<sup>11</sup> The instrumental resolution was of order 2 meV (FWHM) at zero energy transfer.

## 2. Transmission correction

The primary difficulty in all stages of the neutron experiment arose from the fact that indium has an extremely large cross section for absorption of thermal neutrons [115 b at 70 meV (Ref. 10)]. The mean free path of a 14-meV neutron is then 0.13 cm. The large indium capture cross section dominates this result, which is thus essentially identical in  $\text{CeIn}_3$  and  $\text{LaIn}_3$ . We chose the final sample thickness to give  $1/e$  absorption. In order to account for the effect of absorption on our measurement we measured the absorption at  $E_i = E_f = 14, 30,$  and  $40$  meV for  $2\theta = 0$  and with the beam perpendicular to the slab ( $\theta_s = 0$ ); and secondly at  $E_i = 30$  meV,  $2\theta = 22.7^\circ$ , and  $\theta_s = (0, 10, \dots, 90^\circ)$ . The absorption decreased

with  $1/\sqrt{E}$  as expected,<sup>10</sup> and the correct ratio of transmission was observed for two sample thicknesses. The decrease in transmission with angle  $\theta_s$  could be adequately described out to  $\theta_s \approx 65^\circ$  by approximating the transmission as that which would occur for a beam scattering at the middle of an infinitely wide slab of thickness  $t = 0.127$  cm. We have used this approximation in correcting the data as noted below, with the additional feature that we accounted for the dependence of the transmission on initial and final energy. To further minimize transmission effects several runs were performed by freezing the sample angle at  $\theta_s = 0$ . Despite these precautions, variation of transmission with energy and angle undoubtedly contributes somewhat to the error in the results reported below.

### 3. Single-crystal experiments

The single-crystal studies were performed using an incident neutron energy of 14.7 meV, PG monochromator and analyzer crystals, and a horizontal collimation  $40'-40'-20'-40'$ . Two PG filters were used to completely eliminate higher-order reflections. The sample was roughly cylindrical, 1 cm in diameter and 1 cm long. It was placed in a helium-filled aluminum can, mounted in the cryostat and oriented in the  $[01\bar{1}]$  zone for one of the two large grains. Scans along the  $[\zeta\zeta\zeta]$ , and  $[\zeta00]$ , and  $[\zeta\zeta0]$  directions revealed only the expected nuclear and magnetic peaks of the single grain of  $\text{CeIn}_3$ . However, the relative intensities of the various peaks were not predictable, due to the large absorption and irregular geometry of the sample. The single-crystal data reported below concerns mainly the temperature dependence of the intensity in the vicinity of the  $(\frac{1}{2}, \frac{1}{2}, \frac{1}{2})$  reflection and for this situation no transmission correction is necessary.

## III. RESULTS AND ANALYSIS

### A. dc susceptibility

In Fig. 1(a) we display the inverse susceptibility of a section of  $\text{CeIn}_3$  cut from the main boule used in the neutron experiment. The data are in excellent agreement with results reported elsewhere<sup>1,3</sup> confirming the quality of the neutron sample. The susceptibility is seen to be Curie-Weiss-like  $[\chi(T) = C_1/(T + \theta)]$  with a value of  $C_1$  almost equal to the value  $C = 0.807$  emu K/mole expected for free  $J = \frac{5}{2}$  cerium ions. This, along with lattice-constant results,<sup>1,2</sup> confirms the trivalence of the material.

In Fig. 1(b) we plot the dc susceptibility in the vicinity of the  $\text{CeIn}_3$  phase transition. There are two key features of these data: The first is that the max-

imum indicates that the ground state is antiferromagnetic; the second is that at the transition the susceptibility shows an extremely sharp cusp, whereas in most antiferromagnets the transition occurs at an inflection point below the maximum. This latter feature will be discussed further below.

### B. Antiferromagnetic phase transition

#### 1. Determination of the spin structure and the saturation moment

To determine the spin structure in the ordered phase we performed elastic scattering measurements at low temperatures. For  $T = 5$  K peaks corresponding to  $(\frac{1}{2}, \frac{1}{2}, \frac{1}{2})$ ,  $(\frac{3}{2}, \frac{1}{2}, \frac{1}{2})$ , and  $(\frac{3}{2}, \frac{3}{2}, \frac{1}{2})$  reflections appeared. No change in the nuclear scattering (corresponding to a concomitant structural transformation) was seen in the order phase. The three magnetic reflections can be indexed on a doubled chemical cell of cubic symmetry having a lattice constant  $2a_0$ . The spin structure is thus identical to that of the  $\text{AuCu}_3$ -like intermetallic  $\text{DyPt}_3$ .<sup>12</sup> The cerium moments are aligned in opposite directions in adjacent (111) magnetic planes; it is an example of  $(\pi\pi\pi)$  antiferromagnetic order. For powder samples, or for single crystals with equal population of all domains, no information can be obtained on the precise direction of the Ce spins in the (111) planes, due to the cubic symmetry.<sup>10</sup>

The moment was obtained by comparing the integrated intensity of the magnetic peaks to that of the nuclear peaks.<sup>10</sup> In Fig. 2 we show the data for the (1,1,1) and (2,2,0) nuclear reflections and the  $(\frac{1}{2}, \frac{1}{2}, \frac{1}{2})$  and  $(\frac{3}{2}, \frac{1}{2}, \frac{1}{2})$  reflections at 5 K. To determine the integrated area we have drawn a smooth curve through the magnetic peak and through the background and taken the area between. The procedure is only good to 10–20%, given the statistics. The final result is that the ordered moment is  $0.65 \pm 0.1\mu_B$  per cerium atom.

#### 2. Critical behavior near $T_N$

The total intensity  $I$  in the superlattice peak is the sum of two terms: the Bragg scattering intensity  $I_{\text{Br}}$  which is proportional to the square of the staggered magnetization  $M_{\text{st}}^2$ ; and the critical scattering  $I_{\text{cr}}$  which is proportional to the fluctuations in the magnetization. The latter usually becomes large at  $T_N$ . In Fig. 3 we plot  $I(\frac{1}{2}, \frac{1}{2}, \frac{1}{2})$  versus temperature. There are two noteworthy features: First of all the intensity approaches  $T_N$  in nearly linear fashion for  $T < T_N$ ; secondly, the critical scattering, which usually manifest itself as a tailing out of the total intensity, is not visible on the scale of Fig. 3(a). Only when

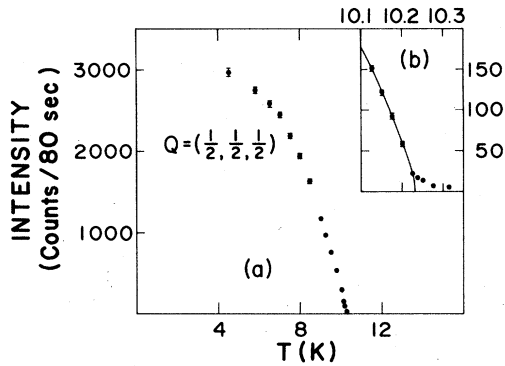


FIG. 3. Peak intensity in the  $(\frac{1}{2}, \frac{1}{2}, \frac{1}{2})$  magnetic superlattice peak vs temperature near  $T_N$  for a single large crystallite of  $\text{CeIn}_3$ . This intensity is proportional to the square of the staggered magnetization. Note the near linearity of approach to  $T_N$ . (b) (Inset) The same scattering on an expanded scale near  $T_N$ . The solid line is a guide to the eye; the deviations from it show the onset of fluctuations in the order parameter.

the region near  $T_N$  is enlarged do the fluctuations become visible [Fig. 3(b)]. As a crude measure of the strength of the fluctuations we note that the ratio  $I(T_N)/I(5)$  is of order half a percent; this is to be contrasted with the more conventional behavior of  $\text{DyPt}_3$  where  $I(T_N)/I(5)$  is 10%.<sup>12</sup>

The near linearity of  $I(T)$  for  $T < T_N$  suggests mean-field behavior. In addition the critical fluctuations seem to be suppressed. For a mean-field transition, the dc susceptibility should show a cusp at  $T_N$ , whereas for normal critical behavior (and Wilson exponents) the derivative  $d(T\chi)/dT$  should diverge at  $T_N$  with a specific-heat exponent [i.e.,  $d(T\chi)/dT \sim |T - T_N|^{-\alpha}$ ] so that  $T_N$  occurs at an inflection point below a rounded maximum.<sup>13</sup> Thus, in most antiferromagnets critical fluctuations round out the maximum in the dc susceptibility. An example of this latter behavior is  $\text{CeAl}_2$ .<sup>14</sup> The cusplike behavior of the dc susceptibility observed in Fig. 1(b) is additional evidence of the suppression of critical fluctuations.

To determine the exponent of the order parameter the critical scattering must be determined and subtracted from the total intensity. In Fig. 4 we plot the intensity versus wave vector in the vicinity of the superlattice peak for four temperatures near  $T_N$ . At 15 K no critical scattering is observed; this establishes the background. At 10.00 K, below  $T_N$ , only Bragg scattering is observed; this establishes instrumental resolution. (The contribution from the critical scattering at this temperature should be of the order of a single count.) At 10.25 K the critical scattering is just visible as a line broadening; at 10.31 K the curve is correspondingly weaker and broader. To estimate the critical scattering  $I_{cr}$  below  $T_N$  we have

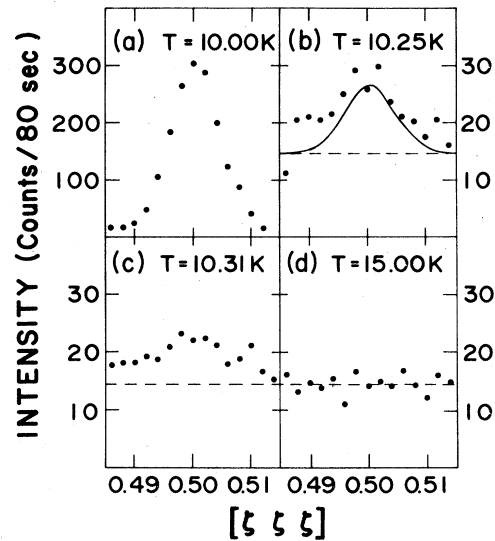


FIG. 4. Scattering from the critical fluctuations in the vicinity of the  $(\frac{1}{2}, \frac{1}{2}, \frac{1}{2})$  superlattice peak near  $T_N$ . (a)  $T = 10.00$  K. This is Bragg scattering and establishes instrumental resolution. (b)  $T = 10.25$  K. The solid line represents instrumental resolution, determined in (a), and the dashed line represents the background. The scattering is just outside instrumental resolution. (c)  $T = 10.31$  K. The half-width has broadened considerably. (d)  $T = 15$  K critical fluctuations are negligible; this establishes the background.

drawn a smooth curve through the data for  $I_{cr}$  above  $T_N$  and extrapolated below  $T_N$  using the mean-field condition that, for  $\epsilon = |T_N - T|/T_N$ , the value of  $I_{cr}(\epsilon)$  for  $T > T_N$  should be twice as large as  $I_{cr}(\epsilon)$  at the same value of  $\epsilon$  below  $T_N$ .<sup>15</sup> Only the two points closest  $T_N$  in Fig. 5 are substantially affected by this subtraction.

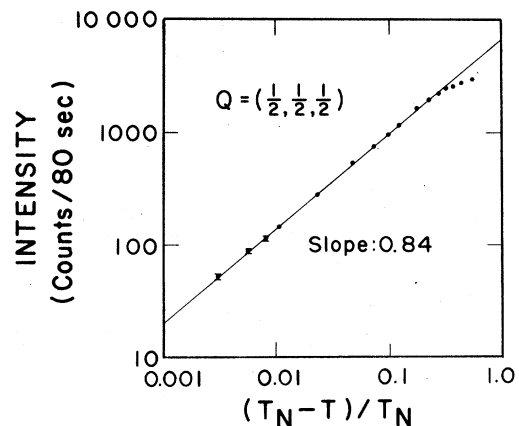


FIG. 5. Plot of the peak Bragg intensity in the  $(\frac{1}{2}, \frac{1}{2}, \frac{1}{2})$  reflection vs  $\epsilon = (T_N - T)/T_N$ . The solid line represents a best fit to Eq. (1); the slope demonstrates that  $2\beta = 0.84$ .

To determine the critical exponent of the order parameter we then least-squares fit the data to the formula

$$M_{st}^2(T)/M_{st}^2(0) = A e^{2\beta} \quad (1)$$

The best values of the parameters are:  $T_N = 10.23 \pm 0.01$ ,  $A = 2.2 \pm 0.2$ , and  $\beta = 0.42 \pm 0.02$ . The fit to the data for these values is shown in Fig. 5. This value of  $\beta$  is too large, in comparison with the expected (Wilson) exponent  $\beta = 0.33$ , although too small for strict mean-field behavior. It is as though the system is in a crossover regime between mean-field and critical behavior.

### C. Spin dynamics

#### 1. Inelastic cross section

In Fig. 6(a) we exhibit the scattered intensity versus energy transfer for  $\text{CeIn}_3$  at 5 K. There is a broad peak centered around 13 meV with a half-width of order 10 meV. This inelastic scattering arises from several sources: magnetic scattering from the cerium 4*f* electrons, phonon scattering from  $\text{CeIn}_3$  and scattering from the aluminum sample holder and room background. To estimate the nonmagnetic contribution to the scattering we have measured the inelastic cross section at 10 and 300 K of a sample of  $\text{LaIn}_3$ , identical in geometry and with the identical sample holder to that used in the  $\text{CeIn}_3$  experiment.  $\text{LaIn}_3$  is isostructural with  $\text{CeIn}_3$ , with very similar lattice constant and atomic weights; furthermore  $\text{CeIn}_3$  is trivalent and shows no lattice-constant or thermal-expansion anomaly<sup>2</sup> so no marked phonon softening is expected; hence (apart from the differing scattering lengths of lanthanum and cerium) the polycrystalline averaged phonon spectra should be essentially identical. Indeed, use of an isostructural nonmagnetic intermetallic compound to estimate the phonon background is standard practice in neutron studies of mixed-valence compounds.<sup>16,17</sup> The results are shown in Fig. 6(b). The nonmagnetic scattering is quite small and featureless.

To estimate the phonon scattering in  $\text{CeIn}_3$  the  $\text{LaIn}_3$  data must be scaled for the different scattering lengths and masses of cerium and lanthanum. Assuming identical phonon densities of states, then at fixed  $Q$ ,  $\omega$ , and  $T$  in the incoherent approximation (valid at large  $Q$ ) the ratio of the phonon scattering in  $\text{CeIn}_3$  to that in  $\text{LaIn}_3$  should be

$$\left( \frac{b_{\text{Ce}}^2}{M_{\text{Ce}}} + \frac{3b_{\text{In}}^2}{M_{\text{In}}} \right) \left/ \left( \frac{b_{\text{La}}^2}{M_{\text{La}}} + \frac{3b_{\text{In}}^2}{M_{\text{In}}} \right) \right. = 0.6 \quad (2a)$$

On the other hand, in the limit of small  $Q$  the ap-

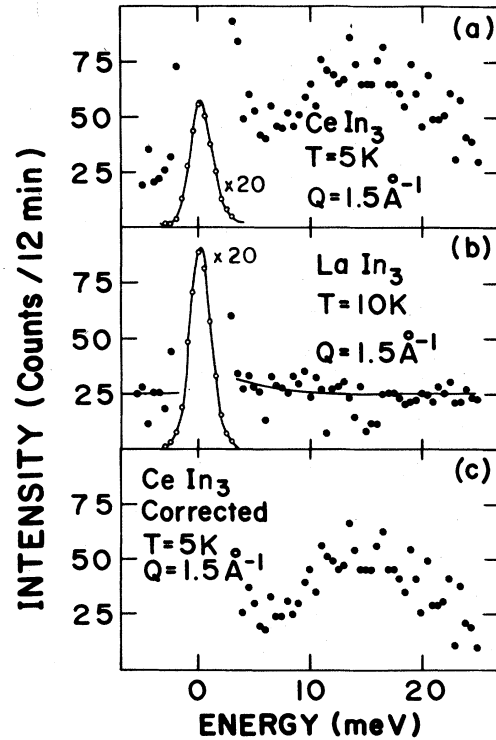


FIG. 6. (a) Scattering intensity vs energy loss for polycrystalline  $\text{CeIn}_3$  for  $T = 5$  K and  $Q = 1.5 \text{ \AA}^{-1}$ . (b) Scattering intensity vs energy loss at 10 K for a  $\text{LaIn}_3$  sample with identical geometry and sample holder; this establishes the nonmagnetic scattering in (a). The solid line was chosen as a smooth approximation to the data; the solid line for negative energy establishes the background. (c) Magnetic scattering in  $\text{CeIn}_3$ , obtained by scaling the smooth curve of part (b) for thermal occupation and scattering lengths, and subtracting from the data of (a).

propriate ratio (coherent scattering) is

$$\left( \frac{b_{\text{Ce}}}{\sqrt{M_{\text{Ce}}}} + \frac{3b_{\text{In}}}{\sqrt{M_{\text{In}}}} \right)^2 \left/ \left( \frac{b_{\text{La}}}{\sqrt{M_{\text{La}}}} + \frac{3b_{\text{In}}}{\sqrt{M_{\text{In}}}} \right)^2 \right. = 0.67 \quad (2b)$$

Since these two results are virtually identical we have chosen 0.6 as the scale factor. Hence to determine the magnetic scattering we first subtracted the background (as determined from energy-gain data at low temperatures) and then the phonon scattering (scaled for scattering lengths using Eqs. (2) and scaled for temperature using the Bose factor  $[n(\omega) + 1]$ ). The results at 5 K are shown in Fig. 6(c). Finally we corrected the results for finite transmission using the assumption outlined above. The results for  $Q = 1.5 \text{ \AA}^{-1}$  and four temperatures are shown in Fig. 7.

It is seen from Fig. 6 that the magnetic scattering dominates the phonon scattering at the small  $Q$  value ( $1.5 \text{ \AA}^{-1}$ ) studied; the phonon scattering makes only a small contribution above background between 0

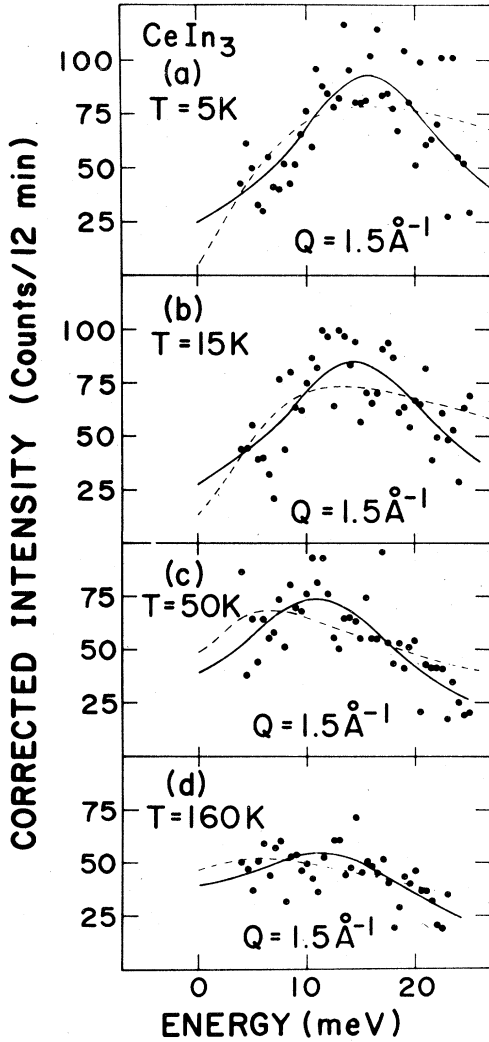


FIG. 7. Magnetic scattering intensity vs energy loss for  $\text{CeIn}_3$  for  $Q = 1.5 \text{ \AA}^{-1}$  and four temperatures. (The data have been corrected for the variation of transmission with energy transfer.) The dashed lines represent the best fits of the data to the quasielastic cross section, Eqs. (3) and (4). The solid lines represent best fits to the Lorentzian cross section, Eq. (5), with parameters given in Table I. (a)  $T = 5 \text{ K}$ , (b)  $T = 15 \text{ K}$ , (c)  $T = 50 \text{ K}$ , and (d)  $T = 160 \text{ K}$ .

and 10 meV, while most of the magnetic scattering is at higher energies. Hence the final result is insensitive to the details of the phonon subtraction procedure. As an additional check that the  $\text{CeIn}_3$  scattering is primarily magnetic at  $Q = 1.5 \text{ \AA}^{-1}$ , we measured the  $Q$  dependence of the scattering at  $\Delta E = 13 \text{ meV}$  and  $T = 150 \text{ K}$ . When the phonon  $Q$  dependence, as determined from a similar measurement for  $\text{LaIn}_3$ , was subtracted out, the resulting scattering was found to decrease with  $Q$  in a manner consistent with the  $J = \frac{5}{2} 4f$  form factor. We also measured the inelastic scattering at  $T = 15 \text{ K}$  and

$Q = 3.0 \text{ \AA}^{-1}$ ; it was reduced in intensity from the  $Q = 1.5 \text{ \AA}^{-1}$  data by a factor approximately equal to the ratio of the form factors, but otherwise identical.

## 2. Analysis in terms of quasielastic and displaced Lorentzian cross sections

In general the scattering from a magnetic system is given by<sup>18</sup>

$$I(Q, \omega) \propto |f(Q)|^2 [n(\omega) + 1] \text{Im}\chi(Q, \omega), \quad (3)$$

where  $f(Q)$  is the form factor for the magnetic ion and  $\chi(Q, \omega)$  is the dynamical susceptibility which contains the essential physics of the problem. We now assume that the dynamical susceptibility is  $Q$ -independent and the only  $Q$  variation of the intensity is due to the form factor. To further analyze our data we least-squares fit our results to two different forms of  $\text{Im}\chi(\omega)$ . In one case we assume that the scattering is totally due to relaxational processes such that the susceptibility is of quasielastic form

$$\text{Im}\chi(\omega) = A\Gamma\omega/(\omega^2 + \Gamma^2), \quad (4)$$

where  $\Gamma$  is the inverse of a characteristic relaxation time. This form of the cross section has been found to be valid for the mixed-valent materials  $\text{Ce}_{1-x}\text{Th}_x$  (Ref. 16) and  $\text{CePd}_3$  (Ref. 17). If  $\hbar T \gg kT$  then  $I(Q, \omega)$  will exhibit a peak at a finite-energy transfer even though we are dealing with a truly relaxational process. The results of the fit to the corrected data are given as the dotted lines in Fig. 7.

As a second choice for the form of the cross section we assume that the peak represents a broadened crystal-field excitation. For the cubic environment of  $\text{CeIn}_3$  we expect the  $J = \frac{5}{2}$  level of cerium to be split into a  $\Gamma_7$  doublet and a  $\Gamma_8$  quartet.<sup>19</sup> In other cubic cerium intermetallics one typically finds the doublet lowest with a crystal-field splitting  $\Delta/k$  of order 50–100 K. The cross section would then be given by the sum of two delta functions centered at  $\pm\Delta$ , with appropriate Boltzmann factors.<sup>20</sup> To treat the situation of broadened crystal-field excitations, we replace the delta functions by Lorentzians. The resulting form of  $I(Q, \omega)$  is<sup>18</sup>

$$I_{\text{CF}}(Q, \omega) = A \left[ \frac{2}{(2 + 4e^{-\beta\Delta})} \frac{1}{[(\hbar\omega - \Delta)^2 + \Gamma^2]} + \frac{4e^{-\beta\Delta}}{(2 + 4e^{-\beta\Delta})} \frac{1}{[(\hbar\omega + \Delta)^2 + \Gamma^2]} \right]. \quad (5)$$

This form of the cross section should be taken as only approximate. Elastic scattering within the  $\Gamma_7$  and  $\Gamma_8$  multiplets is not included, but should only be important in our measurements at  $T = 160 \text{ K}$ . Also, Eq. (5) is strictly valid only when  $\Delta \gg \Gamma$  such that sharp resonances are present. When  $\Gamma \geq \Delta$  this formalism is no longer valid and one should calculate the dynamical susceptibility by inversion of the com-

TABLE I. Parameters of the least-squares fits of the magnetic scattering of  $\text{CeIn}_3$  (Fig. 7) to the Lorentzian form for the cross section [Eq. (5)].

$T$	$Q$	$A$	$\Delta$	$\Gamma$
5	1.5	8568	15.8	9.6
15	1.5	8960	14.5	10.3
50	1.5	8969	11.0	10.5
160	1.5	10309	11.9	10.9
15	3.0	8583	13.6	11.0

plete dynamical matrix.<sup>21</sup>

The results of the fit to Eq. (5) are shown as solid lines in Fig. 7 and the parameters are listed in Table I. It can be seen from Fig. 7 that at all temperatures Eq. (5) represents the data better than Eq. (4). Several features of the displaced Lorentzian fits are of interest. For  $Q = 1.5 \text{ \AA}^{-1}$  the parameters  $A$  and  $\Gamma$  remain relatively constant, up to 50 K, while  $\Delta$  moves to progressively smaller energies. The constancy of  $A$  and  $\Gamma$  gives added support for the validity of this form for the scattering at low temperatures.

Apart from the poor statistics, a major source of uncertainty in these fits is the choice of transmission correction. The approximation that we used (Sec. IIB2) tends to underestimate the transmission at high angles. In the inelastic scattering this would imply that the corrected data should fall off even faster at high energies than indicated in Fig. 5. This gives added support to the choice of Eq. (5) as the correct cross section.

Our main assertion is that the displaced Lorentzian form for the cross section minimizes the error better, and shows more internal self-consistency than the quasielastic form. It is, of course, entirely reasonable to assume that the correct formula for the cross section would be a combination of the quasielastic and Lorentzian forms: the quasielastic form would represent  $\Gamma_7 \rightarrow \Gamma_7$  and  $\Gamma_8 \rightarrow \Gamma_8$  scattering; and the displaced Lorentzian would represent  $\Gamma_7 \rightarrow \Gamma_8$ ,  $\Gamma_8 \rightarrow \Gamma_7$  scattering. Given the poor statistics and the uncertainty in the correct choice of scattering function for such a strongly damped crystal-field excitation, we have chosen not to attempt a more complicated analysis than that given.

#### IV. DISCUSSION

We have seen that at low temperatures and small  $Q$  the inelastic scattering in  $\text{CeIn}_3$  (Figs. 6 and 7) is dominated by magnetic scattering which is adequately described by a Lorentzian  $A/[(\hbar\omega - \Delta)^2 + \Gamma^2]$ , where  $\Delta$  and  $\Gamma$  are both of order 10 meV (Table I). A na-

tural interpretation is that  $\Delta$  represents the  $\Gamma_7 \rightarrow \Gamma_8$  crystal-field excitation energy of the  $J = \frac{5}{2}$  cerium ion in the cubic environment and that the damping arises from a Kondo-type  $s$ - $f$  exchange coupling which is expected in this trivalent material since the  $4f$  level is presumably not far below the Fermi level.<sup>1</sup> However, given the statistics, we cannot completely rule out that the inelastic magnetic scattering shown in Fig. 7 represents quasielastic scattering with a cross section of the form of Eq. (4). Indeed the most plausible conjecture is that the observed scattering represents a combination of a central quasielastic component due to scattering within the  $\Gamma_7$  doublet and  $\Gamma_8$  quartet, and a broad  $\Gamma_7 \rightarrow \Gamma_8$  transition. However, the main conclusion we wish to draw from the inelastic scattering is that there is an abnormally broad magnetic scattering peak which undoubtedly arises from interactions of the  $4f$  spins with conduction electrons. We stress that  $\text{CeIn}_3$  is believed to be trivalent, and that such a broad feature is unusual in integral-valence rare-earth intermetallics where sharp crystal-field levels are usually observed.<sup>22</sup>

An important piece of information can be extracted from the data of Fig. 7. Namely, if we interpret<sup>1</sup> the half-width ( $\sim 10$  meV) of the broad scattering peak as a measure of the spin-fluctuation energy  $kT_{sf}$  for  $\text{CeIn}_3$  we find that  $T_{sf} \sim 100$  K. As can be seen from Fig. 1 the high-temperature dc susceptibility obeys a Curie-Weiss law with Weiss parameter  $\theta$  on the order of 65 K. This large value of  $\theta$  certainly reflects the presence of fast spin fluctuations, and, as in previously studied mixed-valence materials,<sup>16,17</sup>  $k\theta$  is of the same order of magnitude as the half-width of the inelastic scattering.

Given such a large spin-fluctuation energy, it is surprising that magnetic order occurs, because the strength of the interaction between  $4f$  spins (as measured by  $T_N \sim 10$  K) is an order of magnitude smaller than the coupling to the conduction electrons (as measured by  $T_{sf}$ ) which tends to flip the  $4f$  spins and give rise to a nonmagnetic ground state. In this situation the  $4f$ - $4f$  interaction must act to stabilize the local moment, which is simultaneously being reduced by the  $s$ - $f$  exchange interaction, so that ordering may occur. The situation is analogous to that which is discussed in the Kondo-lattice model<sup>7</sup> which treats ordering of an integral-valence material in the presence of strong  $s$ - $f$  exchange where the  $s$ - $f$  exchange simultaneously compensates the moment and gives rise to the RKKY (Ruderman-Kittel-Kasuya-Yosida) interaction which stabilizes and orders the moment. Two important features of this model are that the ordering should be antiferromagnetic and that the magnitude of the ordered (sublattice) moment should be small. Although it is not clear that this model—which is one-dimensional and which neglects direct valence fluctuations—is relevant to  $\text{CeIn}_3$ , the predicted features may be more general. Indeed, an

RPA (random-phase approximation) treatment of the three-dimensional Anderson lattice<sup>23</sup> shows a general tendency to antiferromagnetic instability.

As we have seen, the spin structure in the ground state of CeIn<sub>3</sub> is simple ( $\pi\pi\pi$ ) antiferromagnetism and the ordered moment is  $0.65 \pm 0.1\mu_B$ . The expected moment for ordering within the  $\Gamma_7$  doublet only is  $0.71\mu_B$ . Given the experimental error in the estimate of the moment, a reasonable interpretation is that the ordering simply occurs within the doublet with no moment reduction due to spin fluctuations. However, the large width of the inelastic cross section suggests that there are abundant low-energy excitations of the spins, of the form  $\Gamma_7 \rightarrow \Gamma_8$ , and  $\Gamma_7 \rightarrow \Gamma_7$  even for  $T < T_N$ . This makes it unlikely that a static ordered  $\Gamma_7$  moment would survive. Indeed, for such a large  $s$ - $f$  interaction one expects hybridization of the  $\Gamma_7$  and  $\Gamma_8$  levels. While the situation seems fairly complicated, it is reasonable to infer that the observed small saturation moment represents not simply crystal-field splitting, but a combination of crystal-field and spin-fluctuation effects.

There are two distinct features of the critical behavior which are possibly associated with the strong spin fluctuations. The first is the weakness of the critical scattering. Intuitively we would argue as follows: Critical scattering is connected with the presence of large, long-lifetime critical fluctuations, which would here correspond to large regions of spins arrayed in antiferromagnetic fashion. The fast intrinsic spin fluctuations, due to the strong  $s$ - $f$  exchange coupling, would flip the spins in such a region, tending to reduce the size and lifetime of the critical fluctuations. Thus the critical scattering might appear much broader than in ordinary phase transitions, and indeed might be so broad as to merge into the background, which would be consistent with the observed critical scattering.

The second distinct feature is the nearly mean-field critical behavior—i.e., the large exponent  $\beta = 0.42$  (Fig. 5) which is quite unusual for antiferromagnets. It is reasonable to guess that it is connected with the strong spin fluctuations. In fact, there exists recent theoretical work concerning “quantum critical phenomena,” defined as critical phenomena for systems with  $T_c$  much smaller than characteristic microscopic energies. The basic idea, originally proposed by Béal-Monod<sup>8</sup> for paramagnon systems, is that for such quantum critical behavior the frequency dependence enters the Landau functional in such a way as to effectively increase the spatial dimensionality of the system. Hence the upper marginal dimensionality  $d^*$  (defined such that for  $d > d^*$  Landau theory is valid for all  $T$ ) is no longer four, but takes the value  $d^* = 4 - z$ . Hertz carried through this proposal<sup>9</sup> and showed that  $z$  depended on the details of the dynamics; he found that  $z = 3$  for itinerant ferromagnets and  $z = 2$  for itinerant antiferromagnets. For a  $T = 0$

phase transition, in a three-dimensional system, mean-field behavior would result. For finite temperatures, however, the sample is effectively finite in the extra dimensions, so that when the coherence length grows larger than the effective finite sample lengths in the extra dimensions, the system reverts to three-dimensional behavior; i.e., there is a crossover from quantum (mean-field) to ordinary classical<sup>24</sup> critical behavior (Wilson exponents).

The observed critical behavior in CeIn<sub>3</sub> may very well represent such an effect. The Néel temperature is an order of magnitude smaller than the relevant characteristic energy  $T_{sf}$ . The critical exponent  $\beta = 0.42$  is midway between the Wilson value and the mean-field value. The interpretation, then, is that for the temperature interval studied ( $0.001 < \epsilon < 0.1$ ) the system is in a crossover region between quantum and classical three-dimensional critical behavior. If experiments could be performed at smaller values of  $\epsilon$ , it would be expected that the classical three-dimensional exponents would assert themselves.

## V. CONCLUSION

The neutron studies of CeIn<sub>3</sub> have indeed given microscopic confirmation for the simultaneous role of spin fluctuations, magnetic order, and possibly crystal fields. The interplay is quite fascinating: in one interpretation the  $s$ - $f$  exchange causes a broadening of the crystal-field excitation which is unusually large for an integral-valence rare-earth intermetallic; the crystal-field and the spin fluctuations both act to cause a reduction of the ordered moment; and the spin fluctuations have a marked effect on the critical behavior, causing it to be nearly mean field.

*Note added in proof.* Since completion of this work, two papers have appeared which reproduce some of the present experimental results: A. Benoit *et al.*, Solid State Commun. **34**, 293 (1980) and W. Gross *et al.*, Z. Phys. B **37**, 123 (1980).

## ACKNOWLEDGMENTS

This work was carried out while one of us (J.L.) was a participant in the Brookhaven Summer Program; he would like to express his appreciation to the Brookhaven staff for its hospitality during this period. Work at Brookhaven was supported by the Division of Basic Energy Sciences, U. S. DOE, under Contract No. DE-AC02-76CH00016; work at Irvine was supported by the National Science Foundation through Contract No. DMR79-06578. We are indebted to Marty Blume, Seb Doniach, M. T. Béal-Monod, and John Hertz for useful discussions on this subject. We are grateful to Boyce Grier and Ron Parks for providing the single crystal of CeIn<sub>3</sub> used in part of this study, and to Bob Youngblood who assisted in the data analysis.

- <sup>1</sup>Jon Lawrence, Phys. Rev. B 20, 3770 (1979).
- <sup>2</sup>J. R. Harris and G. V. Raynor, J. Less Common Met. 9, 7 (1965).
- <sup>3</sup>T. Tsuchida and W. E. Wallace, J. Chem. Phys. 43, 3811 (1965).
- <sup>4</sup>K. H. J. Buschow, H. W. de Wijn, and A. M. van Diepen, J. Chem. Phys. 50, 137 (1969).
- <sup>5</sup>S. Nasu, A. M. van Diepen, H. H. Neumann, and R. S. Craig, J. Phys. Chem. Solids 32, 2773 (1971).
- <sup>6</sup>A. M. van Diepen, R. S. Craig, and W. E. Wallace, J. Phys. Chem. Solids 32, 1867 (1971).
- <sup>7</sup>R. Jullien, J. N. Fields, and S. Doniach, Phys. Rev. B 16, 4889 (1977).
- <sup>8</sup>M. T. Béal-Monod, Solid State Commun. 14, 677 (1974); M. T. Béal-Monod and K. Maki, Phys. Rev. Lett. 34, 1461 (1975).
- <sup>9</sup>John A. Hertz, Phys. Rev. B 14, 1165 (1976).
- <sup>10</sup>G. E. Bacon, *Neutron Diffraction* (Oxford University Press, London, 1975).
- <sup>11</sup>N. J. Chesser and J. D. Axe, Acta Crystallogr. Sect. A 29, 160 (1973).
- <sup>12</sup>G. Arnold and N. Nereson, J. Chem. Phys. 51, 1495 (1969).
- <sup>13</sup>M. E. Fisher, Philos. Mag. 7, 1732 (1962).
- <sup>14</sup>I. Zorić, J. Markovics, L. Kupferberg, M. Croft, and R. D. Parks, in *Valence Instabilities and Related Narrow Band Phenomena*, edited by R. D. Parks (Plenum, New York, 1977), p. 479.
- <sup>15</sup>S-K Ma, in *Modern Theory of Critical Phenomena* (Benjamin, New York, 1976).
- <sup>16</sup>S. M. Shapiro, J. D. Axe, R. J. Birgeneau, J. M. Lawrence, and R. D. Parks, Phys. Rev. B 16, 2225 (1977).
- <sup>17</sup>E. Holland-Moritz, M. Loewenhaupt, W. Schmatz, and D. K. Wohlleben, Phys. Rev. Lett. 38, 984 (1977).
- <sup>18</sup>W. Marshall and S. W. Lovesey, *Theory of Thermal Neutron Scattering* (Oxford University Press, London, 1971).
- <sup>19</sup>T. Murao and T. Matsubara, Prog. Theor. Phys. 18, 215 (1957).
- <sup>20</sup>K. C. Turberfield, L. Passell, R. J. Birgeneau, and E. Bucher, J. Appl. Phys. 42, 1746 (1971).
- <sup>21</sup>K. W. Becker, P. Fulde, and J. Keller, Z. Phys. B 28, 9 (1977).
- <sup>22</sup>*Crystal Field Effects in Metals and Alloys*, edited by A. Furrer (Plenum, New York, 1977).
- <sup>23</sup>P. Riseborough and D. L. Mills (unpublished).
- <sup>24</sup>“Classical” is used here in the sense of classical statistics as opposed to quantum statistics. That is, classical exponents are Wilson exponents, quantum exponents are mean field. This follows Ref. 9.